Characteristics and analysis of a turbulent offset jet including the effect of density and offset height

Ali Assoudi [a], Amani Amamou [a], Nejla Mahjoub Saïd [b,c,*], Hervé Bournot [d]

[a] LGM, National Engineering School of Monastir, University of Monastir, Tunisia

[b] Department of Physics, Faculty of Science for Girls, King Khalid University, Abha, Saudi Arabia

[c] LGM, Preparatory Institute for Engineering Studies, University of Monastir, Tunisia

[d] Aix Marseille Univ, CNRS, IUSTI, Marseille, France

* Corresponding author

E-mails: nejla.mahjoub@fsm.rnu.tn, mahjoub_nejla@yahoo.fr

***Abstract*:** This paper presents the results of measurements and numerical predictions of 3D turbulent offset jet flows. Mean velocity and turbulence characteristics of a rectangular offset jet with different offset heights and within variable densities are experimentally and numerically investigated in detail. Four jet gas exit densities, ρ_j = 1.2, 1.25, 1.3, and 1.4, and four offset heights, h/w = 8, 16, 25, and 33, are studied. The considered variation of the jet density is revealed at different Reynolds numbers and the velocity measurements are carried out using a Laser Doppler Velocimetry (LDV) technique. The handled configuration is numerically simulated by solving the Navier-Stokes equations with the finite volume method having a non uniform grid system. Two different closure models are tested: the standard k–ε model and the Reynolds Stress Model (RSM). Results clearly revealed significant effects of the jet density and the offset height on the flow development in the early region. It is noted that the centerline velocity decay increases as the jet density and the offset height increase. It is also observed that the reattachment length of the jet decreases with the increase of the jet density. However, the reattachment length is found to increase with the increase of the offset height.

***Keywords*:** Offset jet, Laser Doppler Velocimetry, Numerical simulation, Offset height, Variable density, Reynolds stresses

NOMENCLATURE

Symbols

D	Mass diffusivity	m^2/s
d_h	Hydraulic diameter	m
g	Gravitational Acceleration	m/s^2
G_k	Term of production due to buoyancy forces	$kg/m.s^3$
h	Offset height	m
k	Kinetic Energy of Turbulence	m^2/s^2
L	Nozzle length	m
P_k	Term of production due to the mean gradients	$kg/m.s^3$
Re	Reynolds number	-
S_{ij}	Mean Strain Rate	-
T	Local temperature	K
T_j	Gaz temperature	K
T_∞	Ambient temperature	K
U_c	Centerline velocity	m/s
U_j	Exit jet velocity	m/s
U_m	Local streamwise maximum mean velocity	m/s
u''	Streamwise turbulence intensity	m/s
$\overline{u_i'' u_j''}$	Reynolds stress	m^2/s^2
u_i, u_j	Velocity components along the i and j directions	m/s
u, v, w	Velocity components along x, y, and z directions	m/s
w	Nozzle width	m
x_{mp}	Rattachement length	m
x, y, z	Cartesian Coordinates	m
y_m	Wall-normal location of U_m	m
$y_{0.5}$	Wall-normal half width	m

Greek Symbols

α	Thermal diffusivity	m^2/s
β	Thermal Expansion Coefficient	-
δ_{ij}	Kronecker symbol (=1 if i=j and 0 if i≠j)	-
ε	Dissipation Rate of the Turbulent Kinetic energy	-
μ	Dynamic Viscosity	kg/m.s
μ_t	Turbulent (or eddy) Viscosity	kg/m.s
ν	Kinematic Viscosity	m^2/s

ρ	Local density	Kg/m^3
ρ_j	Flow ejection density	Kg/m^3
ρ_∞	Ambient density	Kg/m^3

Superscripts

$\bar{}$	Reynolds average
$\tilde{}$	Favre average

1. Introduction

Turbulent offset jet flows are obtained when a jet is discharged into a medium above a wall parallel to the axis of the jet exit but offset by a certain distance. The jet flow may be discharged with a variable density which may be due to temperature variations or variations in the composition by fluids of different density. Given their unique and complex characteristics, offset jets are a prototypical flow configuration to study the physics of complex flow observed in many environmental and engineering applications. For instance, offset jets are relevant in predicting the nature of aircraft exhausts and loading effects of aircraft exhausts on ground structures, in the entrainment and mixing process in gas turbine and boiler combustion chambers, and in energy dissipation devices downstream of hydraulic structures. The offset jet is known to combine the characteristics of free, impingement and wall jets, and it is relatively more complex compared to these types of flows. In fact, based on its flow structure, a turbulent offset-jet can be described by three main regions. Close to the nozzle exit, an offset jet has properties similar to those of a free jet. Then, the entrainment of fluid between the jet, the offset wall and the bottom wall creates a low pressure zone, forcing the jet to deflect towards the wall and eventually attaches to it at the impingement point. This is referred to as the Coanda effect [1]. Furthermore, downstream after the reattachment point, the offset jet has the characteristics of a wall jet flow.

Many parameters can influence the behavior of an offset jet flow. In earlier studies [2-8], the reattachment length has usually been the primary parameter of interest to study the characteristics of an offset jet flow. Previous measurements were made with different techniques such as hotwires, Pitot tubes and Laser Doppler Anemometry (LDA). These studies are mainly concerned with the static pressure distribution and velocities measurements in determining the reattachment length. They developed a more general uniform equation that leads to predict the reattachment length as a function of the offset ratio (d/w). With the technology advancement and the recent discovery of coherent structures in the flow, more researchers shifted their interests to studying these turbulent structures. Wang and Tan [9] presented an experimental investigation of a dual-jet formed by a plane wall jet and a parallel offset jet using the Particle Image Velocimetry (PIV) method. They considered an offset ratio of 2 with a Reynolds number equals to 10^4 based on the single jet width relating to an initial jet velocity of 1 m/s. Dynamic characteristics of the flow, including the Reynolds stresses have been discussed. They observed that the near field of the flow is characterized by a periodic large-scale Karman-like vortex shedding similar to what would be expected in the wake of a bluff body.

Other investigations focused on the effect of the offset ratio (the ratio of the distance from the jet exit to the impingement bottom wall and the jet nozzle diameter). Detailed velocity measurements of 3D offset jets are

carried out by Davis and Winarto [10]. The measurements of mean velocities and turbulence intensities are performed by means of the hotwires technique at a Reynolds number Re=170.000 and with four offset ratios (d/h =0.5, 1, 2 and 4). The authors reported measurements only beyond the reattachment point ($x > x_{mp}$). They found that the displacement of the nozzle from the boundary wall effects the position of the attachment point (x_{mp}). The most comprehensive study of 3D offset jets with various offset ratios was reported by Agelin-chaab and Tachie [11-12]. The authors examined the effects of the offset ratio and Reynolds number on the structure of the turbulent round offset jet using the Particle Image Velocimetry (PIV) at three different Reynolds numbers of 5000, 10,000 and 20,000. They found that the decay and spread rates are nearly independent of the Reynolds number and the offset height.

Nyantekyi-Kwakye et al. [13] presented experimentally the flow characteristics within the recirculation region of the three-dimensional offset jets using a Particle Image Velocimetry technique. Measurements are performed for a rectangular offset jet with four nozzle offset height ratios of 0, 2, 4 and 8. Analysis of the flow field showed that the maximum mean velocity decay rate together with the reattachment length of the jet increased with the increase of the offset height ratio within the recirculation region. The heat transfer characteristics of turbulent offset jet flows are investigated in many papers [14-17]. The effect of different parameters (offset ratio, Prandtl number, Reynolds number and Grashof number) is examined to investigate the flow behavior of conjugate heat transfer. The results are presented in terms of local Nusselt number, local heat flux, wall temperature, and total heat transfer.

Recently, Assoudi et al. [18] derived an experimental and numerical study of a turbulent 3D offset jet discharged into a co-flow stream with different offset and velocity ratios. Measurements data of mean velocities and turbulence characteristics are reported using the Particle Image Velocimetry (PIV). A numerical simulation of the problem is also carried out with the second order turbulent Reynolds Stress Model (RSM). Three velocity ratios $R = u_0/u_\infty$, ($R = \infty$, $R = 1$ and $R > 1$), and two offset heights ($h/d = 5.3$ and 7.8) are investigated to describe the dynamic and turbulent characteristics of the flow. They observed that the increase of the offset ratio gives a better distribution of the jet within the flow field, giving rise to a better dynamic mixture.

Most previous studies are conducted for different values of Reynolds number and offset ratios considered to be of the same fluid property. From this point, the aim of this present paper is to investigate the behavior of a three-dimensional turbulent offset jet injected with different densities issuing into the ambient air at various offset heights (h/w), using a Laser Doppler Velocimetry (LDV) technique (TSI). The specific application for an offset jet with variable densities is to control the rate of the water particles (through the variation of the jet

densities) in order to find solutions that promote the sale of fresh products and fight against food waste. This study is specifically intended to provide experimental data for the development and validation of numerical models. The numerical three-dimensional model is simulated through the resolution of the different governing Navier–Stokes' equations by means of the finite volume method. The effect of the density ratio (ρ_j/ρ_∞) as well as the offset height ratio (h/w) and the distance between the nozzle ejection and impingement surface on the flow structure of 3D offset jets is examined.

2. Experimental facility and measurement method

2.1 *Experimental facility*

The experimental measurements are conducted in a test section of rectangular dimensions 1500 mm, 400 mm, and 400 mm in the longitudinal, vertical and lateral directions, respectively. The side walls were made of smooth acrylic to facilitate the optical access. Fig.1 shows a sketch of the test section of the set up experiment and the cartesian coordinate system used in this study [19]. The jet nozzle is of a rectangular section of length L=60mm and width w=6mm and offset by a height h above the boundary wall. Note that x=0 is at the offset wall containing the jet exit, y=0 is on the surface wall level, and z=0 is the jet symmetry.

2.2 *LDV system and measurement procedure*

In the current study, two method groups are used to investigate the flow structure, namely, the Laser Tomography System employed for the flow visualization and the Laser Doppler Velocimetry (LDV) technique (TSI) performed for the velocity measurements. The jet is formed by an air flow seeded with small particles of water cloud of approximately 3 μm diameter (Nebulization, ARECO®). The Laser tomography is a technique of instantaneous viewing used in analyzing the structure of turbulent flows. It consists of an illumination system (Nd-YAG, 120 mJ/pulse laser of 532 nm wavelength) utilized to illuminate the flow field and a digital camera (Power View 4 M high resolution cross-correlation camera) with a speed of 1280 x1024 pixels CCD used to image the flow field (Fig. 1) . The velocity measurements were carried out by a non-intrusive LDV technique at a point (a small, non-intrusive optical probe volume) defined by the intersection of two laser beams. This technique is based upon a TSI Power View system, including a 120-mJ dual Nd YAG laser, which produces two flat pulses, like PIV system [20, 21]. It also produces of a transmission optics (Bragg cell, beam expanders, beam splitter, prisms, and focusing lens), receiving optics, signal processor units, seeding generation and computer with a data acquisition board and data handling software called "FLOWSIZER". As shown in Fig. 2 the basic

elements of the LDV technique are presented; the Laser Doppler Velocimeter sends a monochromatic laser beam toward the target and collects the reflected radiation. According to the Doppler Effect, the change in wavelength of the reflected radiation is a function of the targeted object's relative velocity. Thus, the velocity of the object can be obtained by measuring the change in the wavelength of the reflected laser light, which is done by forming an interference fringe pattern. The absolute error of the position is very small = 0.1 mm (the LDV probe displacement is done by two optical benches).

2.3 *Test conditions*

The experiments were performed for a rectangular nozzle with an offset height h = 33w. The Reynolds number, which is defined as the ratio of the inertial forces to the viscous forces, is based on the jet exit velocity (U_j) and the jet nozzle Hydraulic diameter (d_h) as Re_j ($U_j d_h/v$) = 2000, 2300, 2600 and 2900. Four different jet density flows ρ_j are tested in the outlet ρ_j = 1.2, 1.25, 1.3 and 1.4. The jet density variation is obtained by changing the water aerosol concentration entrained by the air flow (ARECO®: Air Refreshing Control). Detailed measurements were taken at various locations downstream of the nozzle in the three regions: the reverse flow, impingement and wall jet regions [22]. Two series of a plane offset jet experiments were conducted. The first series was done for the nozzle with an offset height h = 33w and for different jet density flows: ρ_j = 1.2, 1.25, 1.3 and 1.4. The second series of experiments is conducted the jet density ρ_j = 1.3 and for different offset heights: h = 8w, 16w, 25w and 33w.

3. Computational setup

3.1 *Governing equations*

Consideration is given to a steady, three-dimensional, incompressible and turbulent flow. The equations describing this flow are obtained in a system of Cartesian coordinates with the origin located at the intersection of three plans: the vertical plan containing the jet exit (x=0), the ground wall level (y=0) and the symmetry plane (z=0). The choice of the cartesian coordinates system is motivated by the asymmetry of the jet distribution within the domain in spite of the symmetry of the configuration. Once discretized in the cartesian coordinate system, the equation system is written as follows [23]:

$$\frac{\partial \left(\overline{\rho}\,\overline{u}_i\right)}{\partial x_i} = 0 \qquad (1)$$

$$\frac{\partial \left(\bar{\rho}\,\tilde{u}_j\,\tilde{u}_i\right)}{\partial x_j} = -\frac{\partial \bar{p}}{\partial x_i} + \frac{\partial}{\partial x_j}\left(\mu \frac{\partial \tilde{u}_i}{\partial x_j} - \overline{\rho u_i'' u_j''}\right) + \left(\bar{\rho}_\infty - \bar{\rho}\right) g\,\delta_{ij} \tag{2}$$

$$\frac{\partial \left(\bar{\rho}\,\tilde{u}_j\,\tilde{f}\right)}{\partial x_j} = \frac{\partial}{\partial x_j}\left[\left(\frac{\mu}{Sc} + \frac{\mu_t}{\sigma_f}\right)\frac{\partial \tilde{f}}{\partial x_j}\right] \tag{4}$$

Where, $S_c = \dfrac{\nu}{D}$ is the Schmidt number.

In the RANS equations, it appears fluctuating functions and variable terms, such as the Reynolds stress tensor ($\overline{-\rho u_i'' u_j''}$), which are required to be modeled. Therefore, the resolution of this system of equations requires a turbulent closure model able to properly characterize the fluctuating functions. In order to choose the appropriate closure model whose results reproduce the experiments better, the k–ε standard turbulent model and the RSM second-order model are compared. The k–ε standard model is the most widely used for the modeling of turbulent flows. It is the simplest one because it solves two separate transport equations [24].

The Reynolds-Stress Model (RSM) attempts to solve the transport equations for the Reynolds stresses, together with an equation for the dissipation rate. This implies the introduction of several transport equations for all the Reynolds stress components. The RSM model presents the advantage of detailing the three-dimensional aspect of complex flows by computing the destruction of the turbulence through the use of the dissipation rate of the turbulent kinetic energy. The introduction of the RSM model leads to solve the following equation [25]:

$$\underbrace{\frac{\partial}{\partial x_k}\left(\bar{\rho}\,\tilde{u}_k\,\overline{u_i'' u_j''}\right)}_{C_{ij}} = \underbrace{\frac{\partial}{\partial x_k}\mu\frac{\partial}{\partial x_k}\left(\overline{u_i'' u_j''}\right)}_{D_{ij}^L} - \underbrace{\bar{\rho}\left[\overline{u_i'' u_k''}\frac{\partial \tilde{u}_j}{\partial x_k} + \overline{u_j'' u_k''}\frac{\partial \tilde{u}_i}{\partial x_k}\right]}_{P_{ij}} + D_{ij}^T + G_{ij} + \phi_{ij} + \varepsilon_{ij} \tag{7}$$

C_{ij} denotes the convective term and D_{ij}^L, P_{ij}, D_{ij}^T, G_{ij}, φ_{ij}, ε_{ij}, represent respectively, the molecular diffusion, the stress production, the turbulent diffusion, the buoyancy production, the pressure strain and the dissipation rate [26]. The equation of the turbulent kinetic energy (k) and that of the dissipation rate of the kinetic energy (ε) which are relative to the second-order model are defined as follows [27]:

$$\frac{\partial \left(\bar{\rho}\,\overline{u_j}\,k\right)}{\partial x_j} = \frac{\partial}{\partial x_j}\left[\frac{\left(\mu+\mu_t\right)}{\sigma_k}\frac{\partial k}{\partial x_j}\right] + \frac{1}{2}\left(P_{ii}+G_{ii}\right) - \bar{\rho}\,\varepsilon \tag{8}$$

$$\frac{\partial \left(\bar{\rho}\,\overline{u_j}\,\varepsilon\right)}{\partial x_j} = \frac{\partial}{\partial x_j}\left[\frac{\left(\mu+\mu_t\right)}{\sigma_\varepsilon}\frac{\partial \varepsilon}{\partial x_j}\right] + C_{\varepsilon 1}\frac{1}{2}\frac{\varepsilon}{k}P_{ii} - C_{\varepsilon 2}\frac{\bar{\rho}\,\varepsilon^2}{k} \tag{9}$$

3.2 *Flow configuration and boundary conditions*

The computational configuration is summarized in Fig. 3. The jet emitted from a rectangular nozzle with a variable-density discharging into quiescent ambient surroundings with a density ρ_∞=1.2. The nozzle is placed at a bottom distance h=200 mm (33 w), and discharges with a velocity U_j. As illustrated in Fig. 3, the size of the computational domain adopted in this study is 250 w × 66 w × 66 w. The Reynolds number based on the hydraulic diameter jet and the exit velocity is in the range of 2000 to 2900.

A velocity inlet boundary condition is imposed on the jet exit (corresponding to x =0). Various uniform velocities U_j and jet density flows ρ_j were ejected, with a turbulent intensity I=5.3% calculated experimentally. Jets with various densities are obtained by changing the density of the air flow at the nozzle exit. The ideal gas law is applicable and the temperature of the jet T_j is imposed initially by the following relationship: $\rho_j = 1.292\frac{273.15}{T_j}$. Wall functions assumptions are imposed to the impingement wall with zero roughness. The use of this approach (wall function) requires that the first grid point adjacent to the wall is within the logarithmic region: $30< y^+ <100$. At the outlet, along the x and z directions, the boundary zero gradients in the normal direction are prescribed.

3.3 *Numerical method*

The resolution of the above governing equations with appropriate boundary conditions is performed with a numerical code, using the Finite Volume Method (FVM). This method allows the discretization of these equations using the first-order upwind scheme [28]. The SIMPLE algorithm [29] is applied for the pressure–velocity coupling. The equations are solved iteratively using the Tri-Diagonal-Matrix-Algorithm (TDMA). The solution is supposed convergent when the residual value of each variable is less than 10^{-5}.

The resolution of the last equations system requires a very fine meshing in a great part of the domain. In order to describe exactly any dynamic or shear stress variations, particularly near and immediately downstream

the jet, a non-uniform grid was adopted in this study. Furthermore, a sufficiently fine grid is used near the neighboring region of the jet and near the walls (the jet bottom wall and the offset wall) where a very high gradient of variables prevailed in the viscous sub-layer. A three-dimensional grid with 180 × 92 × 76 was elaborated for the computations, which was picked out after a careful grid independence investigation.

4. Results and discussion

4.1 *Flow visualization*

Fig. 4 represents the visualization of the flow progression under the influence of the jet density variation (ρ_j= 1.2, 1.25, 1.3, and 1.4). This figure is actually a sequence of images captured in a series of CCD camera shots on the symmetry plane (z = 0) under the offset ratio of h=33w. It highlights the possibility of free progression of the jet before bending under the influence of the coanda effect. This free progression depends on several factors such as the offset height, the injection ratio and the jet density at the nozzle exit. Referring to Fig. 4, in the case of lighter gases, when the jet density is decreased, the jet is more likely to impose their own behavior which elapses horizontally parallel to the impingement wall before being deflected to the bottom wall. Indeed, this region corresponds to the potential core which is characterized by a similar turbulent mixing as in the free jet flows. Downstream of the nozzle exit, on the outer edge of the jet, it is observed the formation of the ring-like vortices also known as Shear Layer Vortices (SLV). The formation of these vortices is caused by the presence of the Kelvin-Helmholtz instabilities. This phenomenon appears when the flow is subjected to shearing between two fluids which slip one over the other at different velocities. This structure leads to the formation of a "swirling sheet" within the mixing zone when the flow starts to curve towards the impingement surface. Herein, it is noted that the jet increase in width and the fluid is subjected to the effects of the adverse pressure gradient and the strong interaction with the boundary layer. Therefore, the centerline velocity decreases rapidly as it approaches the wall, and the pressure increases inside the jet until it reaches a maximum value at the attachment point. Within the impingement point, part of the inner shear layer fluid is deflected upstream from the attachment point into the recirculation region. This latter consists of an important characteristic; the reattachment length (x_{mp}) which is relevant in determining the development of the flow in this region. The reattachment length was defined as the streamwise distance from the nozzle exit to the point where the jet reattached to the bottom wall. Therefore, the attachment point was estimated as the location on the offset plate above where the reverse flow stops and further downstream, the flow becomes positive. It can be seen that the jet reattaches to the wall at x_{mp}/d_h = 45, 38, 31.8 and 28.2 for ρ_j = 1.2, 1.25, 1.3 and 1.4, respectively. It is observed that the reattachment

length is basically dependent on the jet density, and it decreases with the increase of the jet density. Further downstream in the lighter jet (ρ_j = 1.2 and 1.25), larger structures appear at the upper border of the jet. For the heavier jet these structures seem to have a larger size and the distance between the vortex rings appears to be larger than that observed in the lighter gases.

In Fig. 5, a sequence of images captured under the symmetry plane (z=0) in the case of jet density ρ_j = 1.3 and for different offset ratios (h/w = 8, 16, 25 and 33) is shown. In all the injection cases, the jet emerges and penetrates through the quiescent medium immediately downstream of the nozzle exit. Therefore, the jet is deflected, rolled up and skewed, resulting in the formation of jet Shear Layer Vortices (SLV), which are the result of the Kelvin-Helmholtz instabilities of the annular shear layer that separates from the edge of the jet nozzle. The effect of the offset height is clearly observed in the near-field, which is indicated by the breakdown of the flow after a short distance downstream of the nozzle exit. This breakdown eventually leads to the attachment of the jet to the bottom wall in the impingement point. This latter is clearly seen to increase with the offset height ratio (h/w). The impingement point values (x_{mp}/d_h), obtained from the average of the four approaches, for h/w = 8, 16, 25 and 33 are 9, 11.8, 18.1 and 22.7, respectively. A closer look at the jet in the near-field region shows that the flow is influenced by the variation of the offset ratio. In fact, the recirculation region is greatly reduced when the injected jet location approaches to the impingement plate. Consequently, it is noted a reduction of the size of the upright vortices developed in this region between the jet, the offset wall and the bottom wall.

The mean streamlines and the iso-contours of the mean velocity are shown in Fig. 6, in the symmetry plane (z =0) for the different jet densities (ρ_j=1.2, 1.25, 1.3 and 1.4) and for an offset height h=33 w. The streamlines are plotted to illustrate the main qualitative features of the offset jet flow in the recirculation and development regions. It is clearly shown that the jet entrains an ambient fluid above and below it. From Fig. 6, the jet spreads similarly for all jet density cases. The jet flow maintains its initial velocity value along a particular downstream distance till the potential core is consumed. After that, the jet deflects toward the bottom wall and the velocity decreases with the downstream distance until it reaches zero at the attachment point. Also, it is worth noting that there is a line which takes place beneath the jet and separates the recirculation region within which the streamwise mean velocity is negative. This line is known as ‘the bifurcation line’. Furthermore, it is observed that the bifurcation line decreases in length as the jet density increases. This decrease may be

explained by the larger recirculation zone in the case of lighter jets. On the other hand, Fig. 6 shows a backflow region characterized by the existence of negative streamwise mean velocities. In the two first cases where the jet density is ρ_j=1.2 and 1.25, no sustained recirculation is present. However, the recirculation zone is clearly observed in the two other gas jets (ρ_j=1.3 and 1.4) indicated by the reverse of the streamlines upstream the impingement point. This is due to the short reattachment length in these jets, allowing to a short size of the recirculation zone. These observations reflect previously mentioned deductions about the relation between the jet density and the velocity decay.

4.2 *Computational code validation*

Fig. 7 shows the radial evolution of the streamwise mean velocity (U/U_m) for a gas jet with ρ_j = 1.3, at selected locations as indicated in the figure. These locations are picked out carefully in order to describe the mean flow of the offset jet within the three flow regions; the recirculation region (Fig. 7.a), the reattachment region (Fig. 7. b) and wall jet region (Fig. 7.c). When located within the first region (Fig. 7.a), it is obvious that negative values of mean velocity exist close to the wall in the inner region. This is an indication that the ambient fluid entrains from the wall region into the jet. Besides, it is found that U profiles do not collapse entirely within the recirculation and the development regions (Fig. 7.a, b). This can be attributed to the effect of the jet curvature towards the bottom wall and the strong interaction between the inner and the outer shear layers in the impingement region. Nevertheless, U profiles show a fairly collapse in the outer region. Further downstream, in the wall jet region (Fig. 7.c), axial velocity attains self-similarity at all streamwise locations. Also, it is worth noting that the location of the local maximum value of U shifts downwards from $y_m = 18.18d_h$ at $x/d_h = 5$ in the recirculation region to a constant value of $y_m = 0.9d_h$ in the wall jet region (Fig. 7.c).

In the following, a comparison between experimental data and computational results, carried out by numerical simulation, is reported in Fig. 8 and 9. The K-ε Standard model and the second order RSM model are tested in order to find out which closure model reproduces better the current configuration. Fig. 8 represents the variation of the normalized centerline velocity (U_c/U_j) according to the streamwise locations (x/d_h). A satisfying agreement between numerical and experimental results is obtained for the four studied jet densities (ρ_j = 1.2, ρ_j = 1.25, ρ_j = 1.3 and ρ_j = 1.4). A little discrepancy between RSM and K-ε models is observed in Fig. 8, especially for the three first air densities (ρ_j = 1.2, 1.25 and 1.3). This discrepancy is located in the last flow region showing that the second order RSM model predicts better the jet evolution.

Fig. 9 features the evolution of the normalized longitudinal velocity component (U/U_m) for ρ_j = 1.3, at different streamwise positions along the three regions of the flow. Along downstream locations, U profiles are characterized by a single velocity peak. This peak is shifted close to the bottom wall by going further downstream of nozzle exit ($y_m = 0.9d_h$ at $x/d_h = 55$). Furthermore, the curves did not collapse entirely with the experimental data within the two first zones (recirculation and reattachment regions) whereas a good agreement is noticed beyond the wall jet region ($x/d_h = 32$ and $x/d_h = 55$). This is actually due to the much more turbulent character in the reverse flow zone and the transition of the flow from the impingement region to the wall jet region. Likewise, a good agreement between predicted results obtained with the RSM model and the experimental data is found, as for the centerline velocity decay (Fig. 9). So, the second order closure model RSM is adopted in numerical simulation for the rest of the paper.

4.3 *Effect of density variation*

The development of the mean flow is examined by representing the decay of the centerline velocity (U_c) normalized by the jet velocity (U_j) with the normalized downstream distance x/d_h, for various jet densities and for an offset ratio h/w = 33. Fig. 10, mainly demonstrated the dependence of the centerline velocity decay on the density variation. In fact, immediately downstream of the jet nozzle, there is no interesting difference on the velocity profiles; they collapse reasonably well for all the jet densities. This is explained by the existence of the potential core region in which the velocity along the centerline axis remains constant. Nevertheless, the discrepancy between U_c/U_j curves is clearly observed from the region $x/d_h \geq 20$, where the centerline velocity decay is more rapid for the denser jet than that for lighter gases. At $x/d_h = 48$, for example, $U_c/U_j \approx 0.168$, 0.108, 0.12 and 0, respectively, for ρ_j=1.2, ρ_j=1.25, 1.3 and ρ_j=1.4, indicating that a lighter jet decays more slowly than a heavy one. This is due to the quicker mixing of the heavy jet with the ambient air. This remark is comforted by the fact that "heavy gas tends to mix more rapidly with the ambient air than the lighter gases. This faster mixing of the heavier gas is accompanied by a faster increase of turbulence intensity in the near region (see Fig. 10).

The streamwise mean velocities at different selected locations of the domain are shown in Fig. 11, for different jet densities and for an offset ratio h/w = 33. The definition of these locations is extracted in order to characterize the mean flow within the different regions of the offset jet. At the first position (x/d_h= 9), located in the reveres flow region, it is clear that the mean velocity distribution is independent of the jet density. In fact, the

axial velocity curves collapse reasonably well in this region for all available jet densities. It is also obvious that the velocity profile adopts a Gaussian distribution with a single peak quasi-symmetric relative to the jet-axis. Downstream of the gas injection, the maximum mean velocity decreases with the streamwise distance owing to the deviation of the jet flow towards the wall by the entrainment of the ambient fluid on the jet. Furthermore, y_m moved closer to the bottom wall with increasing the jet density; the heavier is the jet, the faster is its drop. The influence of the jet density appears while moving downstream (at x/d_h=28 and x/d_h=45). Indeed, U profiles do not collapse anymore in the impingement region and in the wall jet region.

For a fixed offset height (h= 33w) and for various gas jet densities, Fig. 12 represents the profiles of the turbulence quantities $\overline{u''u''}$, $\overline{v''v''}$ and $\overline{u''v''}$ at two streamwise locations; x/dh=9 (in the near region) and x/dh=45 (in the far field region). At the first station (x/dh=9), the density variation seems to have a limited effect on the different Reynolds stresses' distributions. The profiles of these quantities are consequently brought together till attaining self-similarity in this region. Nevertheless, the impact of the density variation appears downstream within the wall jet region ($x/d_h \geq 45$) through the increase of the registered peak by increasing the density of considered gases. The maximum level of the $\overline{u''u''}$stress is stronger than the $\overline{v''v''}$component; they have obtained peak values of 0.14 and 0.112 respectively for the denser jet. This implies that the increase in the jet densities allows the increase of the peaks attained by the shear stress component.

4.4 *Effect of offset ratios*

Fig. 13 shows the streamwise mean velocity U, at selected x/d_h locations for different offset ratios using $y_{0.5}$ (the jet half width) as the appropriate length scale for the generic offset jet. Immediately downstream of the jet nozzle, for the locations x/d_h = 2, 4, 7 and 9, there is no interesting difference on the mean velocity profiles: they are similar regardless of the offset ratio differences. Indeed, these profiles depicted the same global behavior in the different x/d_h locations: a Gaussian velocity profile that progressively adopts a peak reached at the position $y = 0.87y_{0.5}$. It is obvious that the jet flow in these positions located at the first region and this peak correspond to the end of the potential core. Far downstream of the jet nozzle, for x/d_h = 45 and 55, we observed that the location of the local maximum velocities decrease with increasing h/w and the location of the peak moves downwards in the wall jet region to a constant value $y = 0.25y_{0.5}$ for h/w = 8 (Fig. 13.a). This is in accordance with values reported in previous observations (Agelin chaab and Tachie, 2011).

The streamwise development of the offset jet flows was characterized using the decay of the maximum streamwise velocity (U_m) and the wall-normal location of maximum velocity y_m (Fig. 14). Previous results as well as those in Davis and Winarto [10] and Chaab and Tachie [11] are considered for comparison. It is obvious, from Fig. 14.a, within the early region of the flow development ($x/d_h \leq 36$), that there is no interesting difference on the U_m profiles: they are similar regardless of the offset heights variation. In fact, the U_m values collapsed reasonably well for all the offset ratios near the nozzle exit. One can also see, from this examination, higher initial decay of the flow close to the nozzle. This indicates a constant U_m within the potential core region for different offset ratios. This observation is consistent with previous measurement results of U_m values. Further downstream in the region $40 \leq x/d_h \leq 80$, the local maximum velocity (U_m) decays monotonically with the streamwise distance, and one can note a little change on the plotted U_m profiles under the different tested offset heights' difference. The development of the location (y_m) with the streamwise distances (x/d_h) for various jets shown in Fig. 14.b, used to exhibit the effects of the offset ratio on the growth of the inner shear layer. It should be noted that the variation of the y_m profiles can occur into three regions: The near region ($x/d_h \leq 20$), which is characterized by the existence of the potential core where y_m remains a constant value. Then, a sharply decrease in the y_m value is clearly identified in the second region ($x/d_h \leq 80$ in the case of h/w = 33). Finally, we note a monotonic increase of y_m in the third region, and that's clearly shown in Fig. 14.b (h/w =8). This indicates that the transition from the second region to the third region is strongly dependent on the offset ratios variation.

The effect of offset height on the Reynolds stresses' distribution are shown in Fig. 15, for the jet density ρ_j=1.3 and within various offset ratios (h/w = 8, 16, 25, and 33). It comes from this examination that the more distinct stress peaks are depicted in the region close to the jet exit; which does not automatically mean higher stress values. Within the first location (x/d_h = 9) for example, we observed that $\overline{u''u''}$ and $\overline{v''v''}$ profiles present double peaks under the lowest offset height which are engendered by the approaching of the jet flow to the impingement wall. Further downstream, at x/d_h = 45, the two shear stress components attain peaks whose magnitudes are comparable for all the last three offset ratios. Moving to the $\overline{u''v''}$ component and within the first jet location, the profiles are going to be reversed, two opposite peaks whose negative magnitudes increase in the vicinity of the bottom wall as we move away from the injection plate. This characterizes the momentum transfer flow between the inner shear layer and the recirculation flow region.

5. Conclusion

The dynamic evolution of three dimensional offset jets under the effect of the density variation and offset ratio on their turbulent behavior is investigated in this paper through experimental and numerical tests. Experimental data are obtained by means of the LDV technique and numerical simulations are performed using the finite volume method together with a turbulent closure model. LDV measurements are conducted for four different Reynolds numbers (based on the jet exit velocity and hydraulic diameter): 2000, 2300, 2600 and 2900. A confrontation between simulated flows and experimental measurements is done using two tested turbulence models, leading to opt for the second order RSM model. Obtained results revealed the presence of a complex resulting flow field. This complexity is shown by the establishment of an elaborated vortical system composed of two main vortices: the recirculation zone vortex structures and the shear layer vortices. In the near jet exit region, the development of the flow is strongly dependent on the jet density and the offset height. The reattachment length is basically dependent on the jet density; it decreases with the increase of the jet density but increases with the offset height. In the early region, no interesting effect of the variation of the density and the offset ratio was observed on the decay of the maximum mean velocities. However, beyond $x/d_h \geq 20$, the decay of the maximum mean velocities was observed to be more affected by the variation in these two parameters. Results also revealed that the analysis of the Reynolds stresses' components are nearly independent of the density variation and the offset height in the near region. Nevertheless, the effect of these parameters is clearly observed in the development region. Indeed, a faster mixing of the heavier gas is accompanied by a faster increase of turbulence.

ACKNOWLEDGEMENTS

The authors would like to express their gratitude to Faculty of Science, King Khalid University, Saudi Arabia for providing administrative and technical support.

References

[1] Tritton DJ. Physical Fluid Dynamics. Von Norstrand Reinhold, UK 1977; 284–286.

[2] Bourque C, Newman BG. Reattachment of a two-dimensional incompressible jet to an adjacent flat plate. Aeronautical Quarterly 1960;11: 201–232.

[3] Sawyer RA. The flow due to a two dimensional jet issuing parallel to a flat plate. J Fluid Mech 1960; 9: 543-561.

[4] McRee DI, Moses HL. The effect of aspect ratio and offset ratio on nozzle flow and jet reattachment. In: Advances in fluids (ed by F.T. Brown). ASME Press, New York 1967; 142-161.

[5] Rajaratnam N, Subramanya K. Plane turbulent reattached wall jets. Journal of the Hydraulics Division 1968; 94: 95-112.

[6] Hoch J, Jiji LM. Theoretical and experimental temperature distribution in two dimensional turbulent jet boundary interaction. J Heat Transfer 1981; 103:331-335. https://doi.org/10.1115/1.3244462

[7] Pelfrey JRR, Liburdy JA. Mean flow characteristics of a turbulent offset jet. Trans ASME J Fluids Eng 1986a; 108:82-88. https://doi.org/10.1115/1.3242548

[8] Nasr A, Lai J. A turbulent plane offset jet with small offset ratio. Exp Fluids 1998; 24:47–57. https://doi.org/10.1007/s003480050149

[9] Wang X, Tan S. Experimental investigation of the interaction between a plane wall jet and a parallel offset jet. Exp Fluids 2007; 42 (4):551-562. https://doi.org/10.1007/s00348-007-0263-9

[10] Davis MR, Winarto H. Jet diffusion from a circular nozzle above a solid plane. J Fluid Mech 1980; 101:201-221. https://doi.org/10.1017/S0022112080001607

[11] Agelin-chaab M, Tachie MF. Characteristics and structure of 3D offset jets. International journal of Heat and Fluid Flow 2011; 32:608–620. https://doi.org/10.1016/j.ijheatfluidflow.2011.03.008

[12] Agelin-chaab M, Tachie MF. Characteristics of turbulent three-dimensional offset jets. Journal of Fluids Engineering 2011; 133(5):1–9. https://doi.org/10.1115/1.4004071

[13] Baafour NK, Shawn PC, Mark FTa, Jarrod M, Getnet M. Flow characteristics within the recirculation region of three-dimensional turbulent offset jet, Journal of Hydraulic Research, 2015;53:2, 230-242. https://doi.org/10.1080/00221686.2014.950612

[14] Heung. BS, Soon.HY, Dae HL. Flow and heat transfer characteristics of a two dimensional oblique wall attaching offset jet. International Journal of Heat and Mass Transfer 2000;43 (13):2395-2404. https://doi.org/10.1016/S0017-9310(99)00312-9

[15] Vishnuvardhanarao E, Das MK. Computation of mean flow and thermal characteristics of incompressible turbulent offset jet flows. Numer Heat Transf Part A 2008;53(8):843–869. https://doi.org/10.1080/10407780701715760

[16] Kanna PR, Das MK. Heat transfer study of two-dimensional laminar incompressible offset jet flows. International Journal of Thermal Sciences 2008; 47:1620–1629. https://doi.org/10.1016/j.ijthermalsci.2008.01.003

[17] Kumar A. Mean flow characteristics of a turbulent dual jet consisting of a plane wall jet and a parallel offset jet. Computers & Fluids 2015; 114: 48–65. https://doi.org/10.1016/j.compfluid.2015.02.017

[18] Assoudi A, Habli S, Mahjoub SN, Bournot H, Le Palec G. Experimental and numerical study of an offset jet with different velocity and offset ratios. Journal of Engineering Applications of Computational Fluid Mechanics 2015; 9(1): 490-512. https://doi.org/10.1080/19942060.2015.1071525

[19] Radhouane Amina, Mahjoub Saïd Nejla, Bournot Philippe. wind tunnel experiments of multijets in crossflow: effect of the injection ratio, Experimental-thermal-and-fluid-science 2019; 105:234-246. https://doi.org/10.1016/j.expthermflusci.2019.04.007

[20] Mahjoub Saïd Nejla, Mhiri H, Le Palec Georges, Bournot Philippe. Experimental and numerical analysis of pollutant dispersion from a chimney. Atmospheric Environment 2005; 39:1727-1738. https://doi.org/10.1016/j.atmosenv.2004.11.040

[21] Radhouane Amina, Mahjoub Saïd Nejla, Mhiri H, Bournot Philippe, Le Palec Georges. Twin inclined jets in crossflow: Experimental investigation of different flow regimes and jet elevations. Environmental Fluid Mechanics 2016; 16:45–67. https://doi.org/10.1007/s10652-015-9410-7

[22] Assoudi A, Habli S, Mahjoub SN, Bournot H, Le Palec G. Three-dimensional study of turbulent flow characteristics of an offset plane jet with variable density. Heat Mass Transfer 2016; 52 (11):2327-2343. https://doi.org/10.1007/s00231-015-1750-9

[23] Bhouri Baouab I., Radhouane Amina, Mahjoub Saïd Nejla, Mhiri H., Bournot P., Le Palec G. Assessment of a chimney jet flowing around an obstacle. Heat Transfer Engineering 2012; 33(10):1–22. DOI: 10.1080/01457632.2012.654451

[24] Nejla Mahjoub Saïd, H. Mhiri, Hervé Bournot, Georges Le Palec., Experimental and numerical modelling of the three-dimensional incompressible flow behaviour in the near wake of circular cylinders, Journal of Wind Engineering & Industrial Aerodynamics, 2008; 96:5, 471-502. https://doi.org/10.1016/j.jweia.2007.12.001

[25] Mahjoub Saïd Nejla, Mhiri H., El Golli S., Le Palec Georges, Bournot Philippe. Three-dimensional numerical calculations of a jet in an external cross flow: application of dispersion of pollutants, Journal of Heat Transfer. Transactions of the ASME 2003; 125, 1-13. https://doi.org/10.1115/1.1560158

[26] Rim Ben Kalifa, Sonia Ben Hamza, Nejla Mahjoub Saïd, HervéBournot. Fluid flow phenomena in metals processing operations: Numerical description of the fluid flow field by an impinging gas jet on a liquid surface, International Journal of Mechanical Sciences 165 (2020) 105220. https://doi.org/10.1016/j.ijmecsci.2019.105220

[27] Ben Kalifa Rim, Nejla Mahjoub Saïd, Hervé Bournot, Georges Le Palec, Effect of nozzle-to-plate spacing on the development of a plane jet impinging on a heated plate, Heat Mass Transfer, 2017; 53: 1305–1314. https://doi.org/10.1007/s00231-016-1904-4

[28] Amani Amamou, Nejla Mahjoub Saïd, Philippe Bournot, Georges Le Palec; Computational study of mass and heat transport in a counterflowing turbulent round jet. Applied Thermal Engineering 2016; 105:25, 724-736. https://doi.org/10.1016/j.applthermaleng.2016.03.090

[29] Ali Assoudi, Nejla Mahjoub Saïd, Hervé Bournot, Georges Le Palec, Comparative study of flow characteristics of a single offset jet and a turbulent dual jet, Heat Mass Transfer 2019; 55:4, 1109–1131, DOI: 10.1007/s00231-018-2493-1.

Figure Captions List

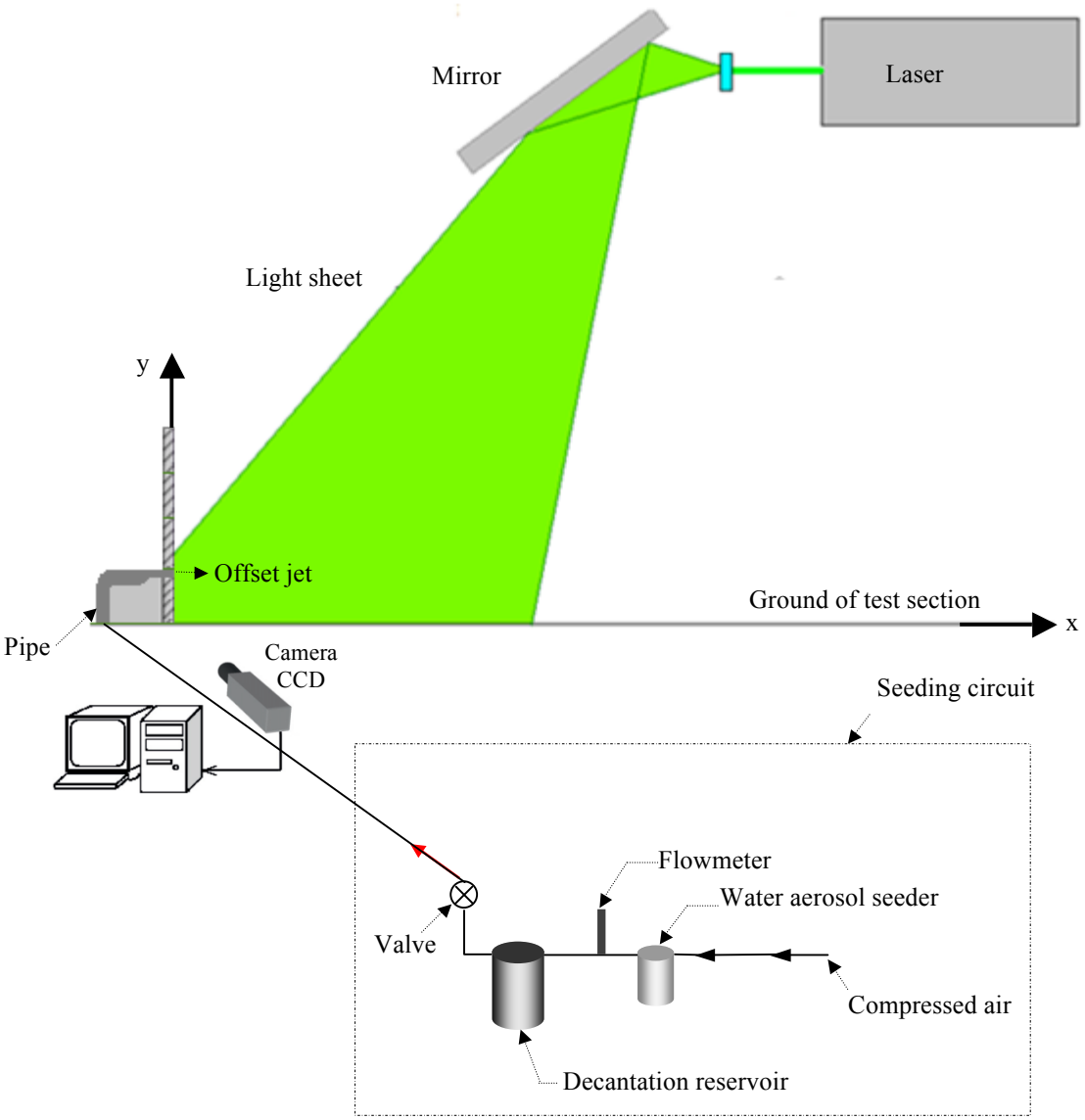

Fig. 1. Experimental setup

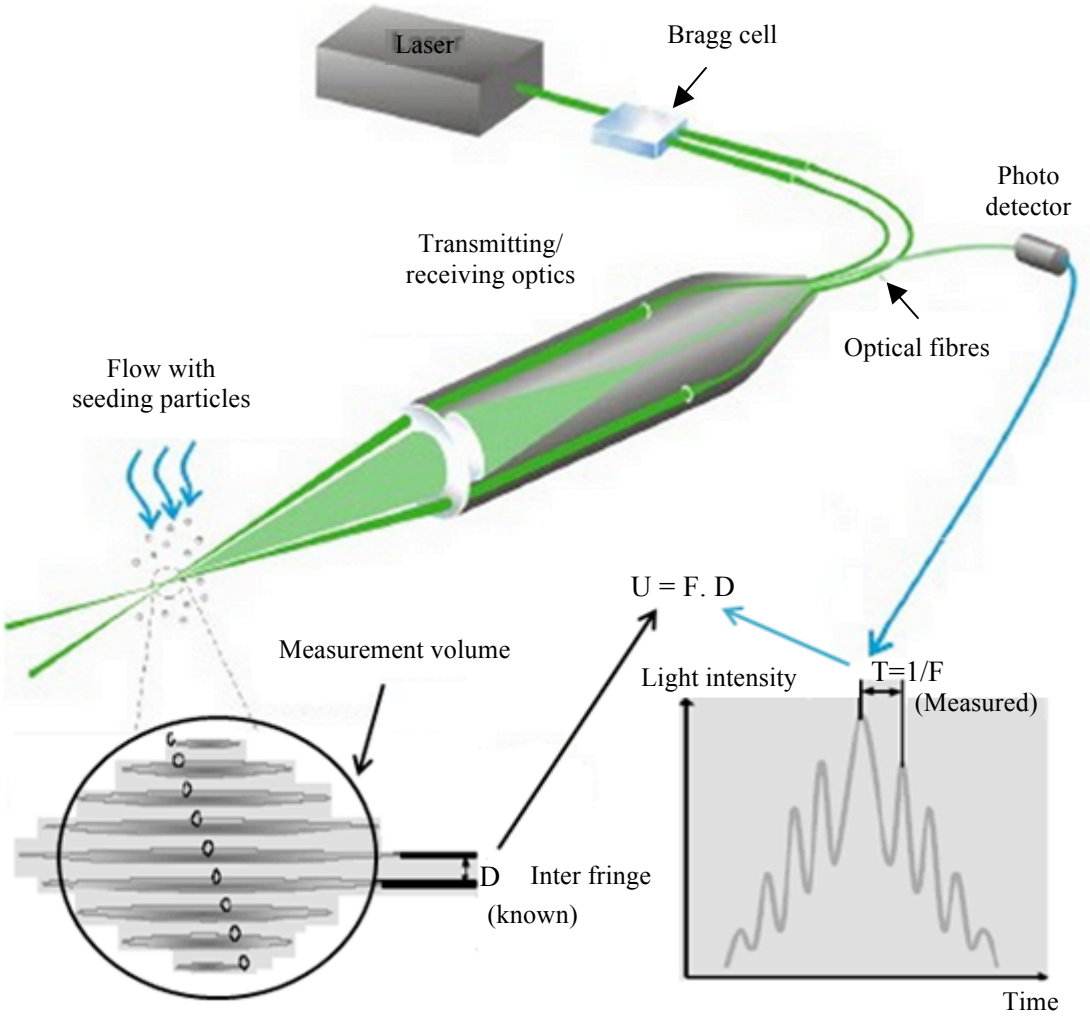

Fig. 2. LDV technique measurements.

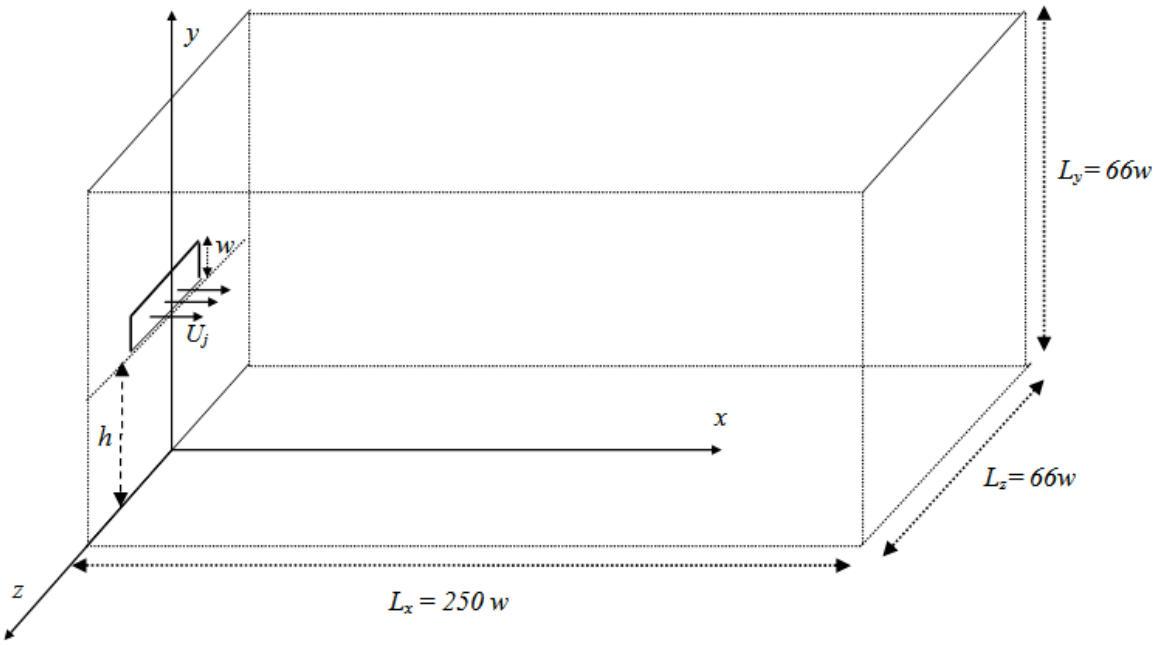

Fig. 3. Geometric configuration of the offset jet.

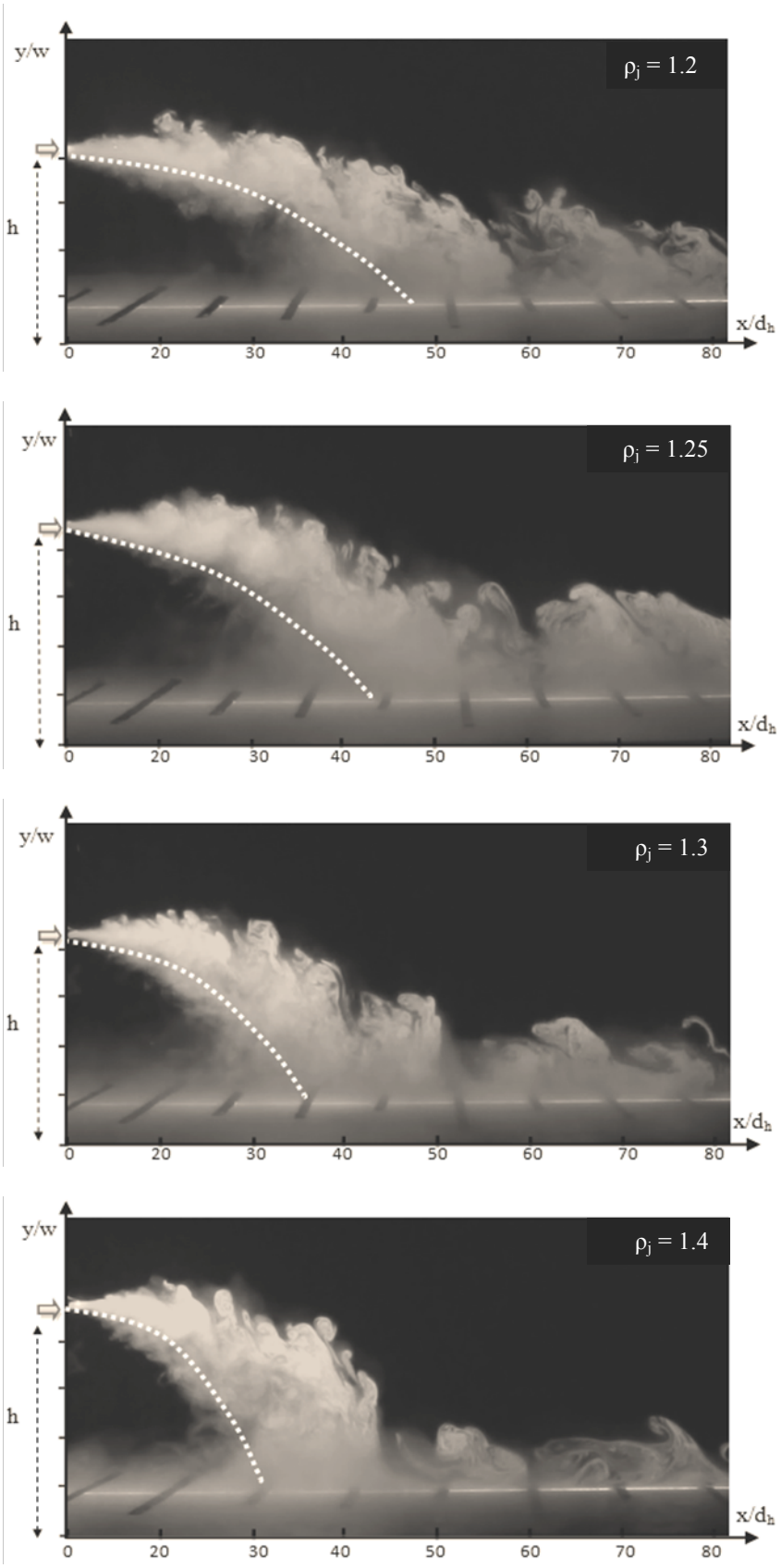

Fig. 4. Evolution of the flow field in the symmetry plane (z = 0) near the jet exit for different densities.

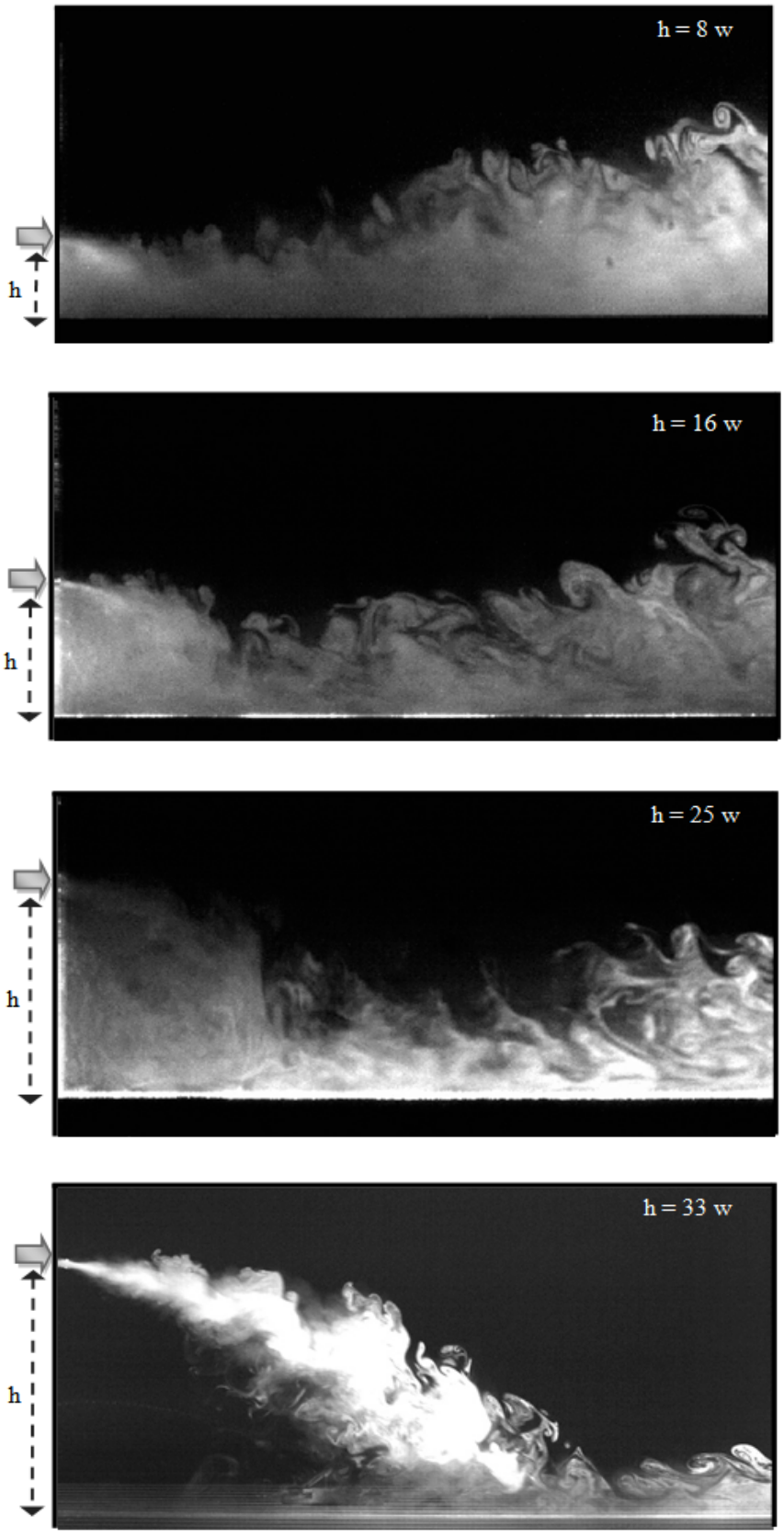

Fig. 5. Flow visualization in the symmetry plane near the jet exit region for different offset ratios.

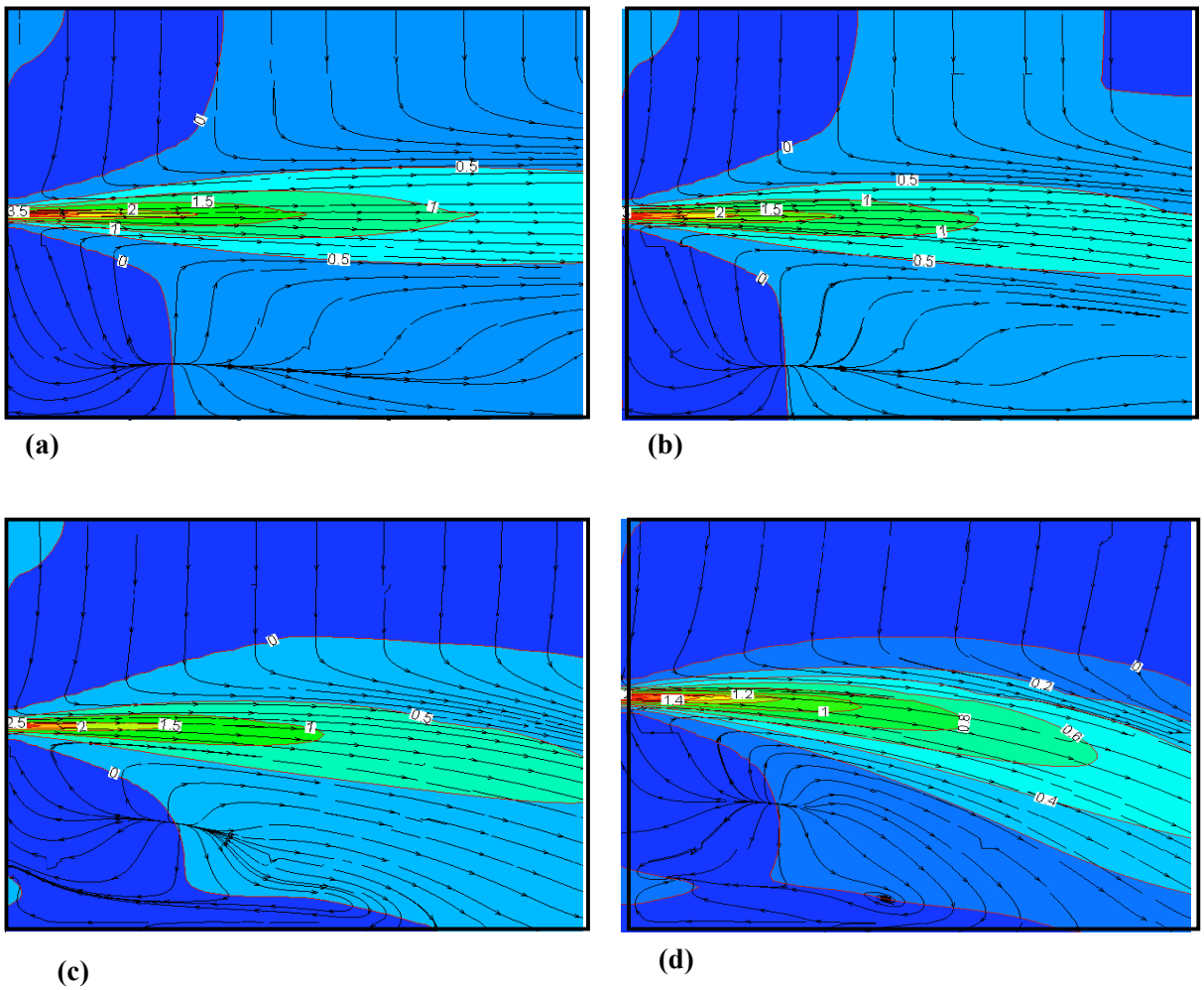

Fig. 6. Mean streamlines and iso-contours of (a–d) mean velocities for different density gases: (a) $\rho_j = 1.2$, (b) $\rho_j = 1.25$, (c) $\rho_j = 1.3$ and (d) $\rho_j = 1.4$ ($h/w = 33$).

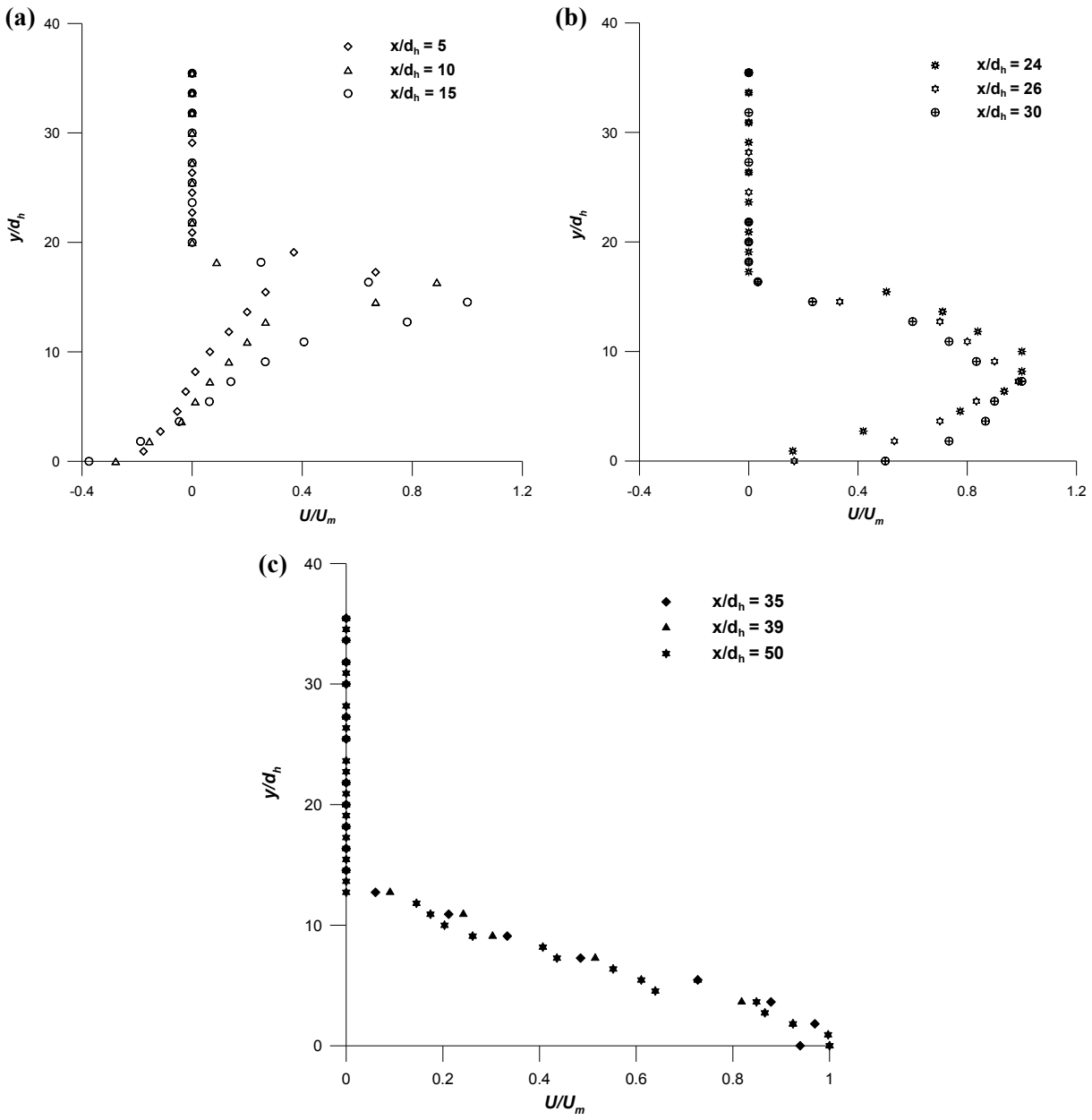

Fig. 7. Profiles of streamwise mean velocities, U, of the offset jet for gas density $\rho_j = 1.3$.

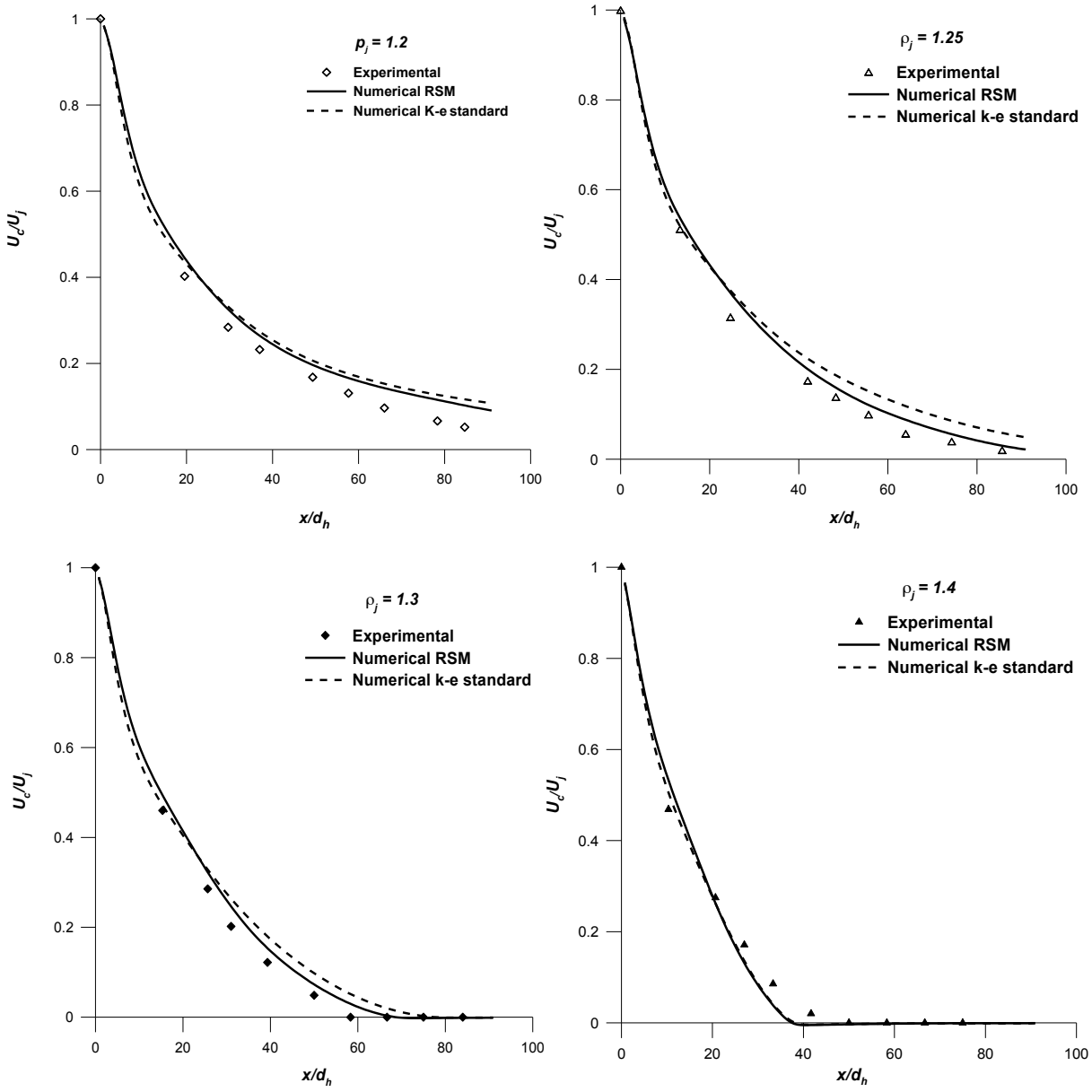

Fig. 8. Mean streamwise velocity along the jet axis for different density jet.

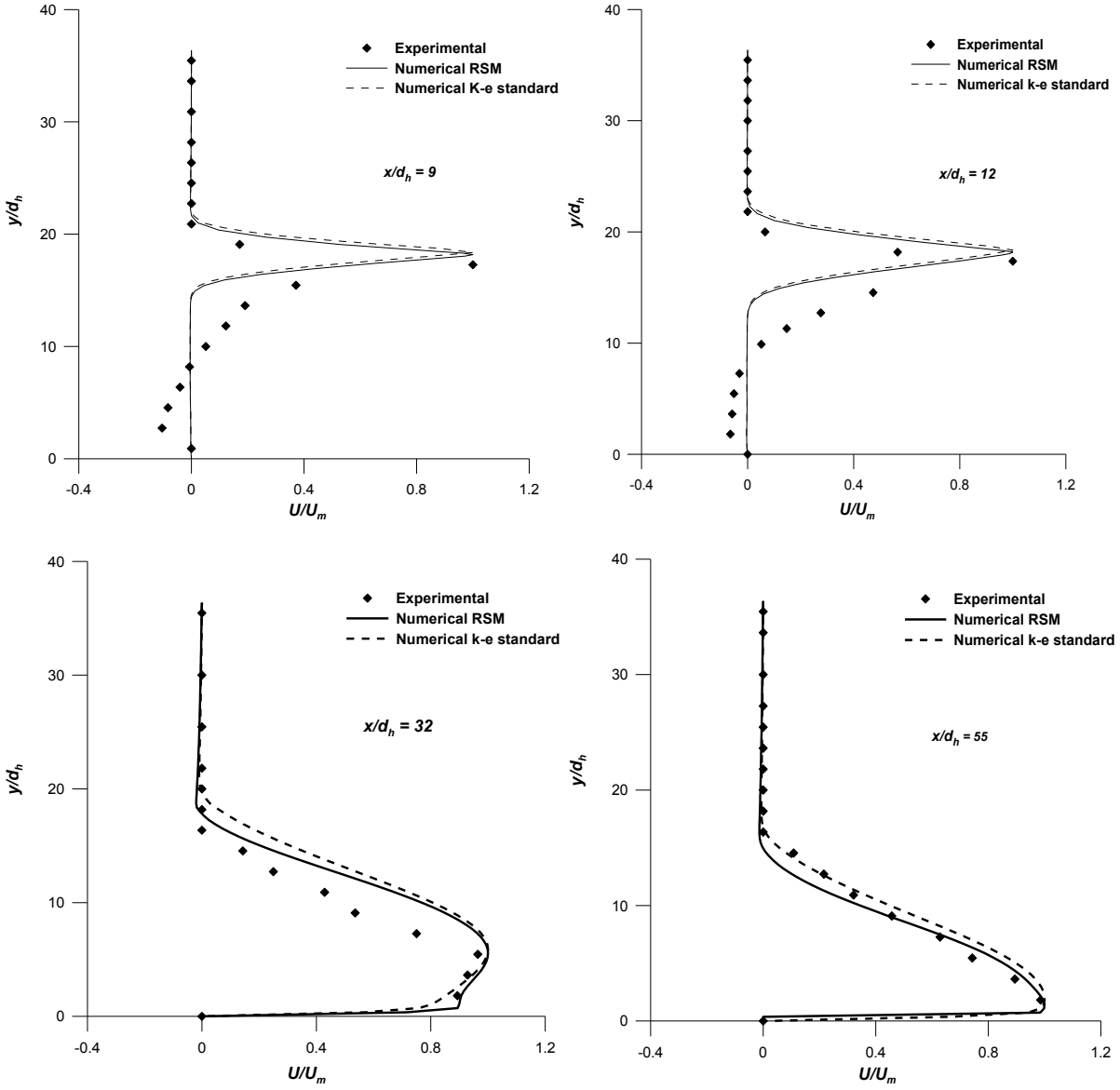

Fig. 9. Profiles of the streamwise mean velocities at different selected positions for density jet $\rho_j = 1.3$.

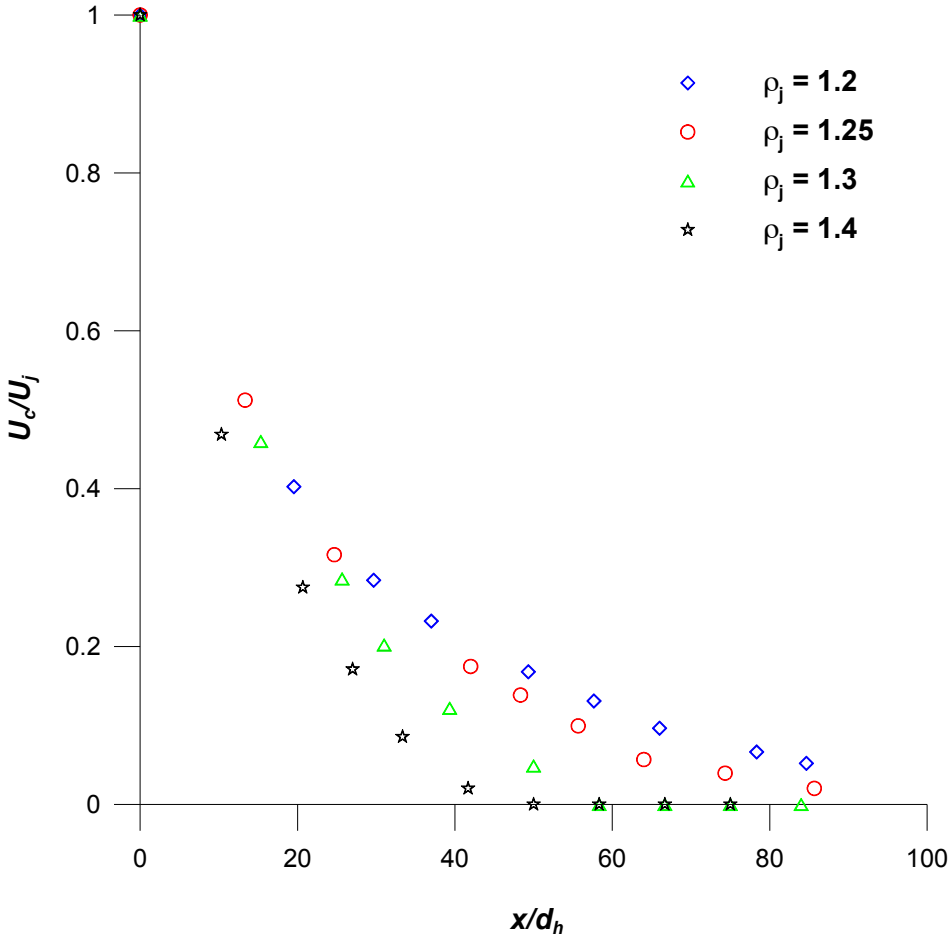

Fig. 10. Centerline velocity decay for different density jet.

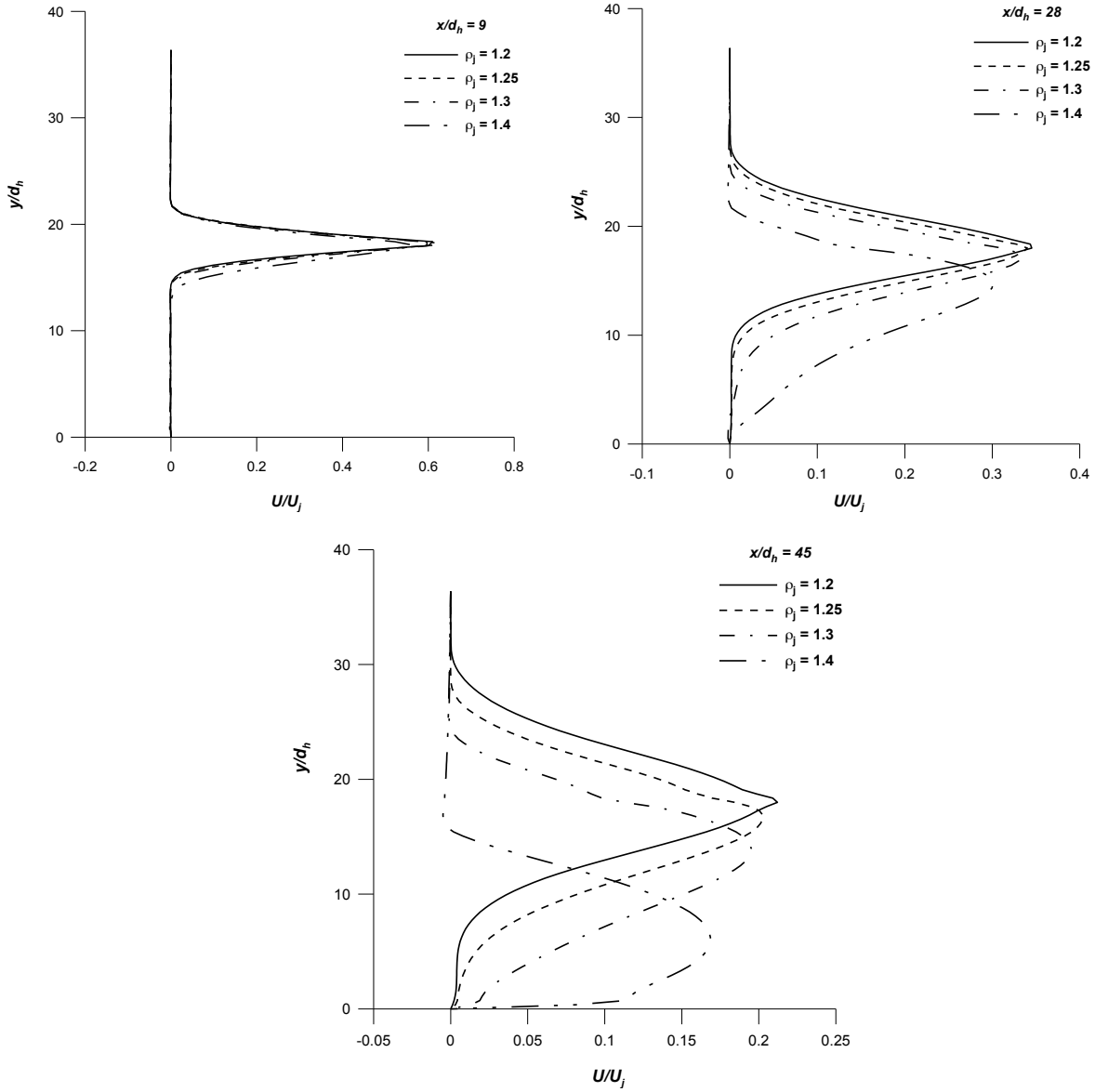

Fig. 11. Streamwise mean velocity distribution of the offset jets for different jet densities at different longitudinal locations of the domain.

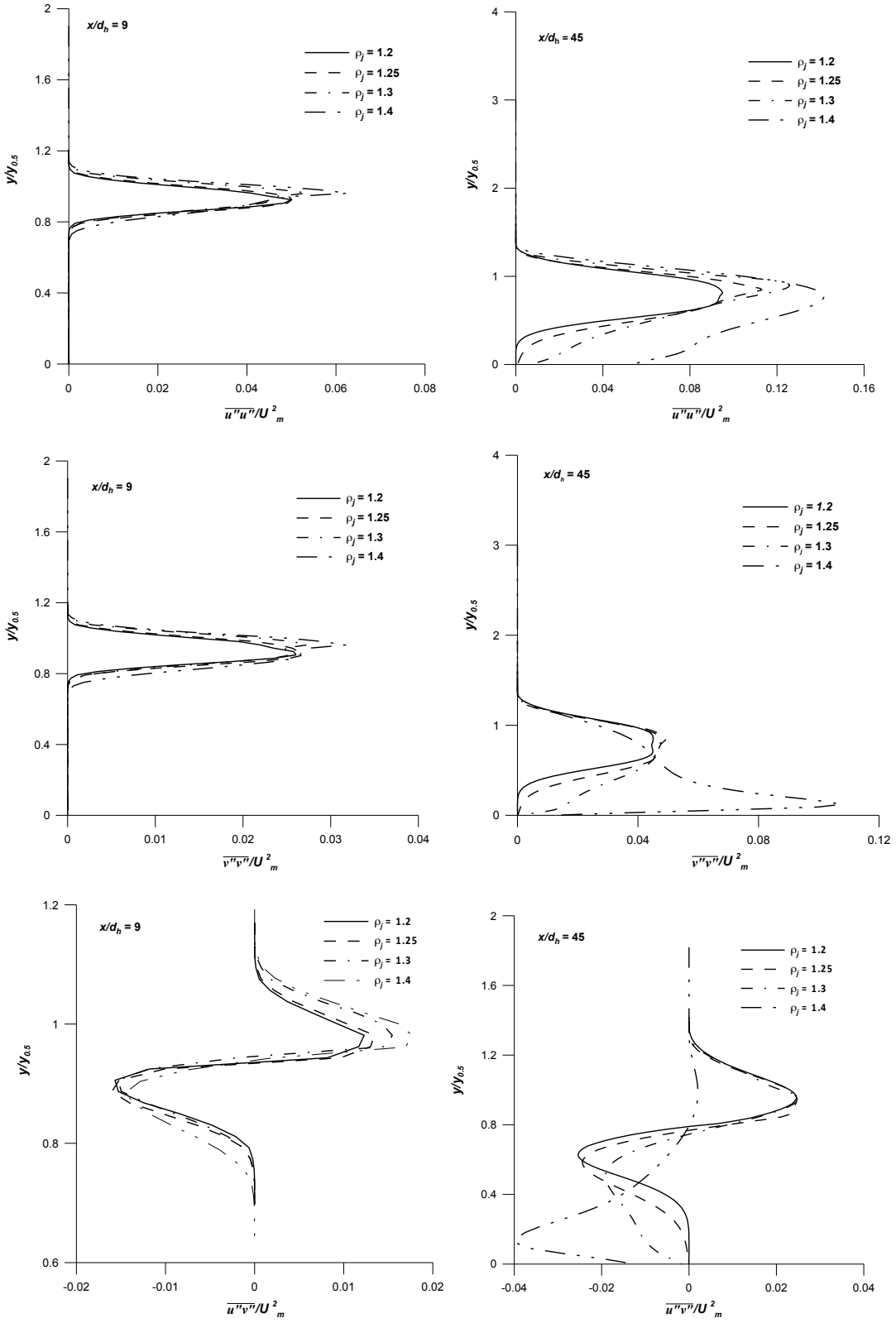

Fig. 12. Comparison of the Reynolds stress distribution for variable densities jet for offset ratio *h/w* = 33.

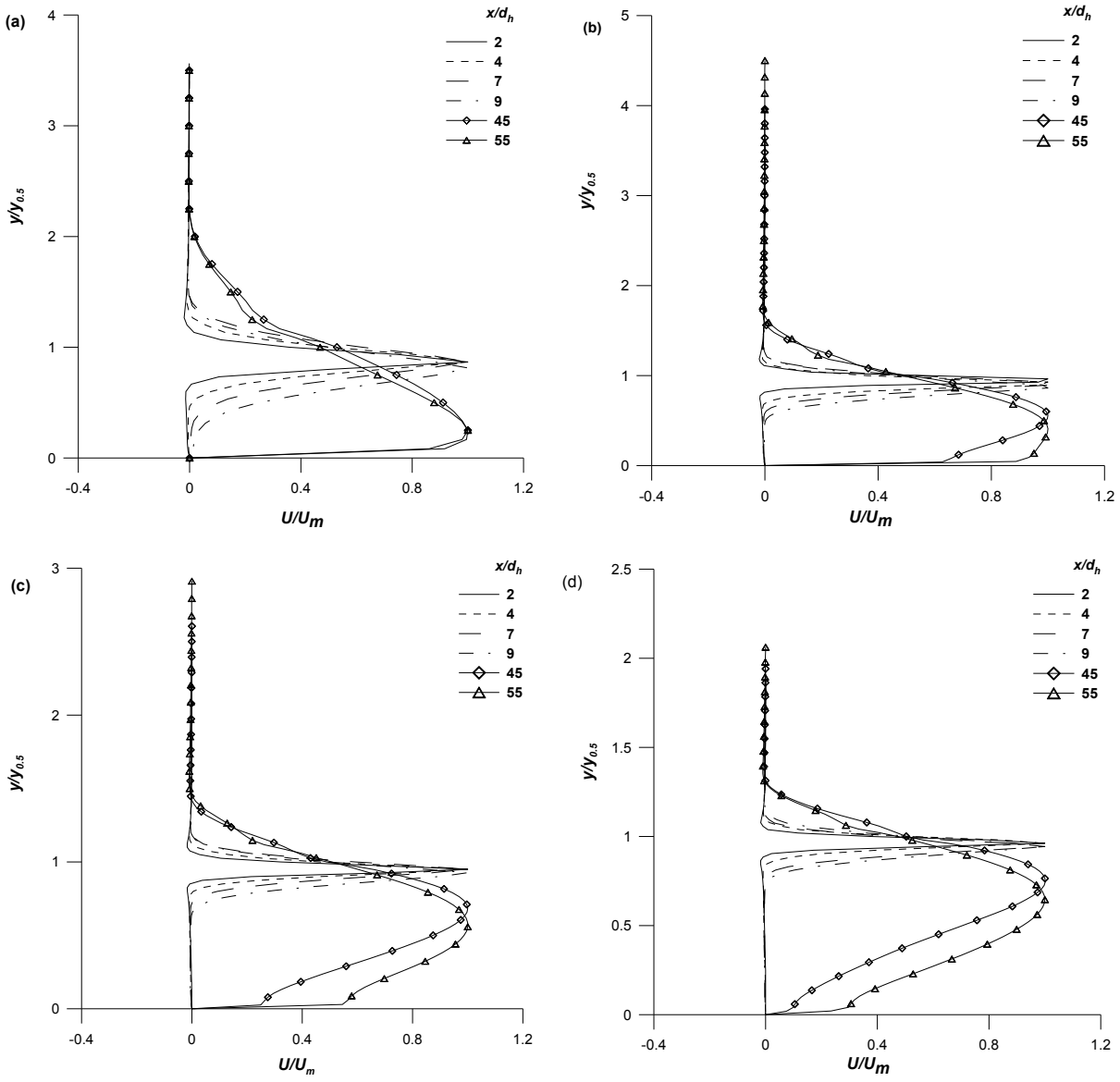

Fig. 13. Streamwise mean velocity distribution of the offset jets for different offset ratios: (a) *h/w* = 8, (b) *h/w* = 16, (c) *h/w* = 25 and (d) *h/w* = 33 (ρ_j = 1.3).

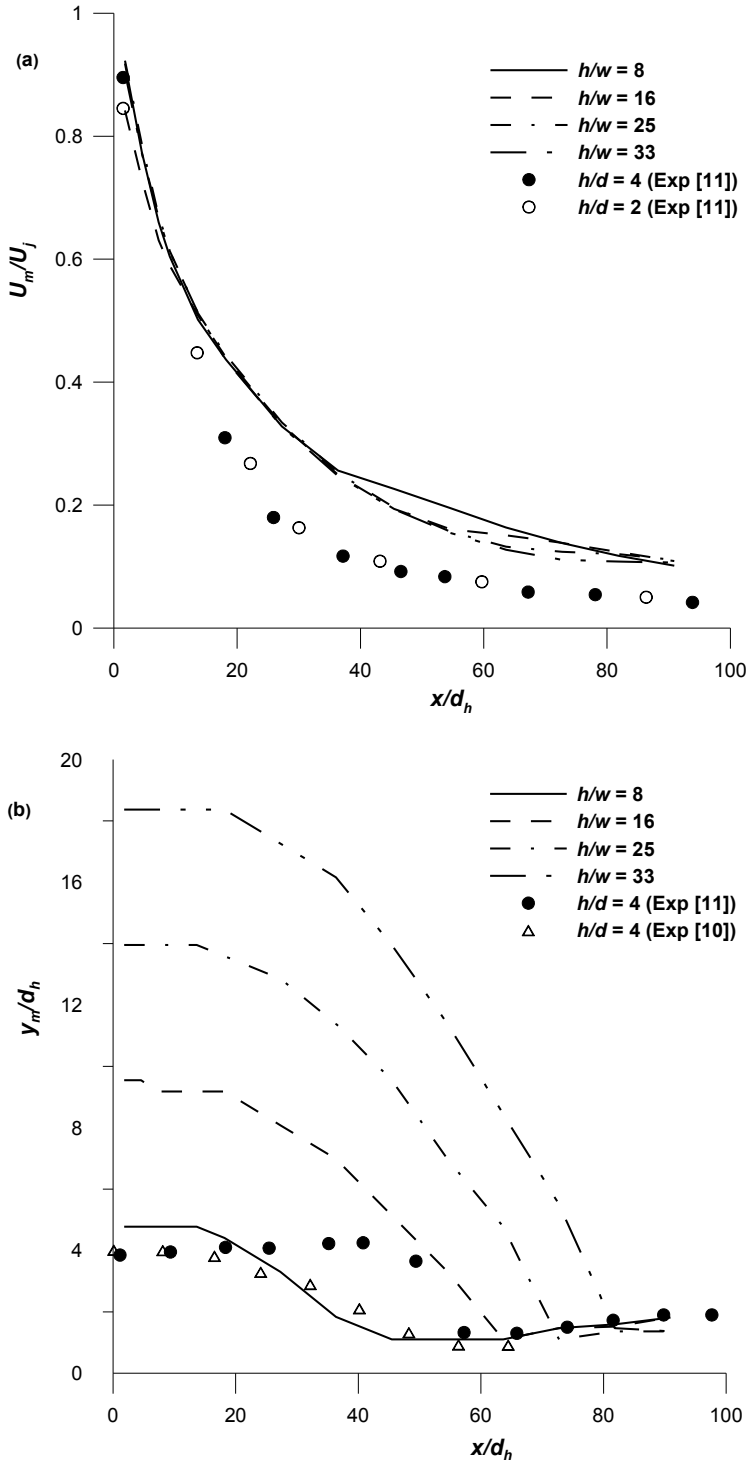

Fig. 14. Variation of **(a)** local maximum mean velocity U_m, **(b)** location of U_m and y_m within different offset ratios (ρ_j = 1.3).

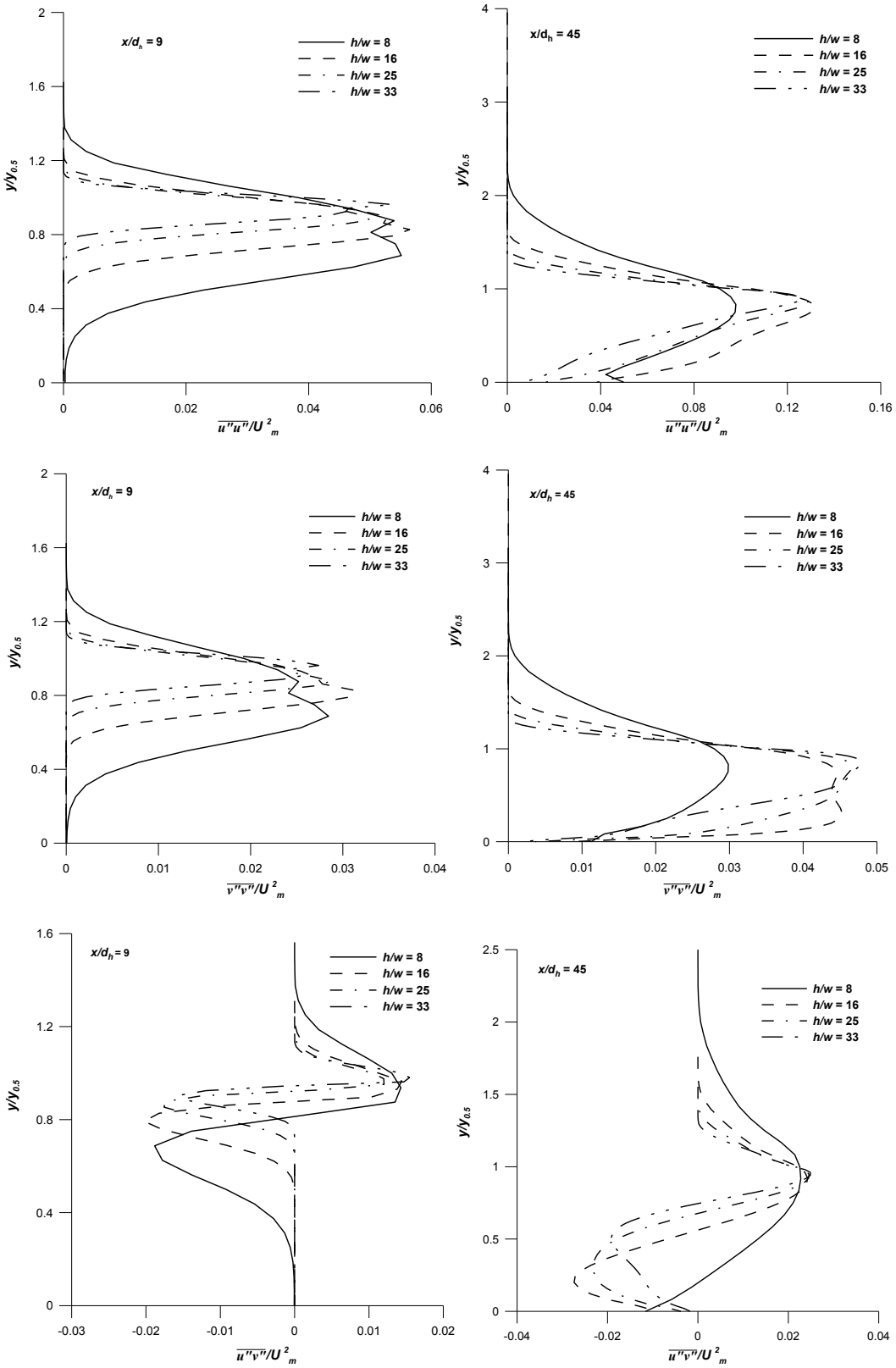

Fig. 15. Comparison of the Reynolds stress distribution for various offset ratios for density jet $\rho_j = 1.3$.